Glucose-Fueled Peptide Assembly: Glucagon Delivery *via* Enzymatic Actuation

Sihan Yu,[1] Sijie Xian,[1] Zhou Ye,[1] Irawan Pramudya,[1] Matthew J. Webber[1,*]

[1]- University of Notre Dame, Department of Chemical & Biomolecular Engineering, Notre Dame, IN 46556 USA

*- mwebber@nd.edu

ABSTRACT: Nature achieves remarkable function from formation of transient, non-equilibrium materials realized through continuous energy input. The role of enzymes in catalyzing chemical transformations to drive such processes, often as part of stimuli-directed signaling, governs both material formation and lifetime. Inspired by the intricate non-equilibrium nanostructures of the living world, this work seeks to create transient materials in the presence of a consumable glucose stimulus under enzymatic control of glucose oxidase. Compared to traditional glucose-responsive materials, which typically engineer degradation to release insulin under high-glucose conditions, the transient nanofibrillar hydrogel materials here are stabilized in the presence of glucose but destabilized under conditions of limited glucose to release encapsulated glucagon. In the context of blood glucose control, glucagon offers a key antagonist to insulin in responding to hypoglycemia by signaling the release of glucose stored in tissues so as to restore normal blood glucose levels. Accordingly, these materials are evaluated in a prophylactic capacity in diabetic mice to release glucagon in response to a sudden drop in blood glucose brought on by an insulin overdose. Delivery of glucagon using glucose-fueled nanofibrillar hydrogels succeeded in limiting the onset and severity of hypoglycemia in mice. This general strategy points to a new paradigm in glucose-responsive materials, leveraging glucose as a stabilizing cue for responsive glucagon delivery in combating hypoglycemia. Moreover, compared to most fundamental reports achieving non-equilibrium and/or fueled classes of materials, the present work offers a rare functional example using a disease-relevant fuel to drive deployment of a therapeutic.

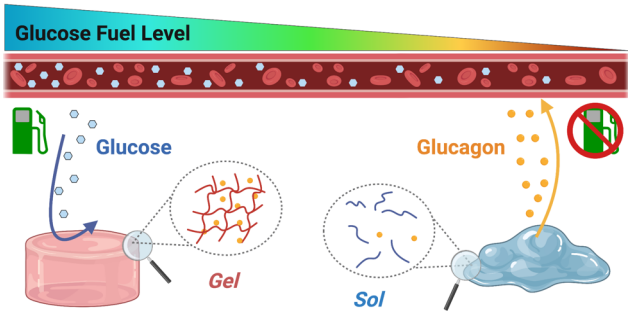

KEYWORDS: self-assembly, supramolecular chemistry, drug delivery, biomaterials, diabetes

INTRODUCTION

Toward the creation of materials for more precise drug delivery, stimuli-responsive strategies have been a topic of extensive focus.[1,2] The use of disease-relevant proteins or analytes to prompt drug release from a circulating nanocarrier or localized depot affords opportunities for improved spatiotemporal control of therapeutic action.[3] Blood glucose management in diabetes presents one circumstance where temporal control of therapeutic bioavailability is particularly relevant.[4–6] In pursuit of high-fidelity blood glucose control, most approaches have focused on engineering glucose-responsive release and/or activity of insulin to replace its deficient or defective signaling and combat hyperglycemia.[7] However, the clinical use of insulin poses substantial risk of overdose. The average person with diabetes has 1-2 serious hypoglycemic episodes each year;[8] most such episodes are attributed to excessive insulin activity. Severe hypoglycemia at night is especially common in children and can prove lethal if not corrected quickly, thus referred to as "dead-in-bed" syndrome.[9] Accordingly, insulin is dosed conservatively and even underdosed in many cases, thereby preferencing chronic health complications from blood glucose instability and hyperglycemia in order to avoid the acute risks of hypoglycemia. Glucagon functions in the healthy endocrine system as an antagonist to insulin by raising blood glucose upon hypoglycemia and, as such, is an interesting therapeutic target.[10] Integrating glucose-

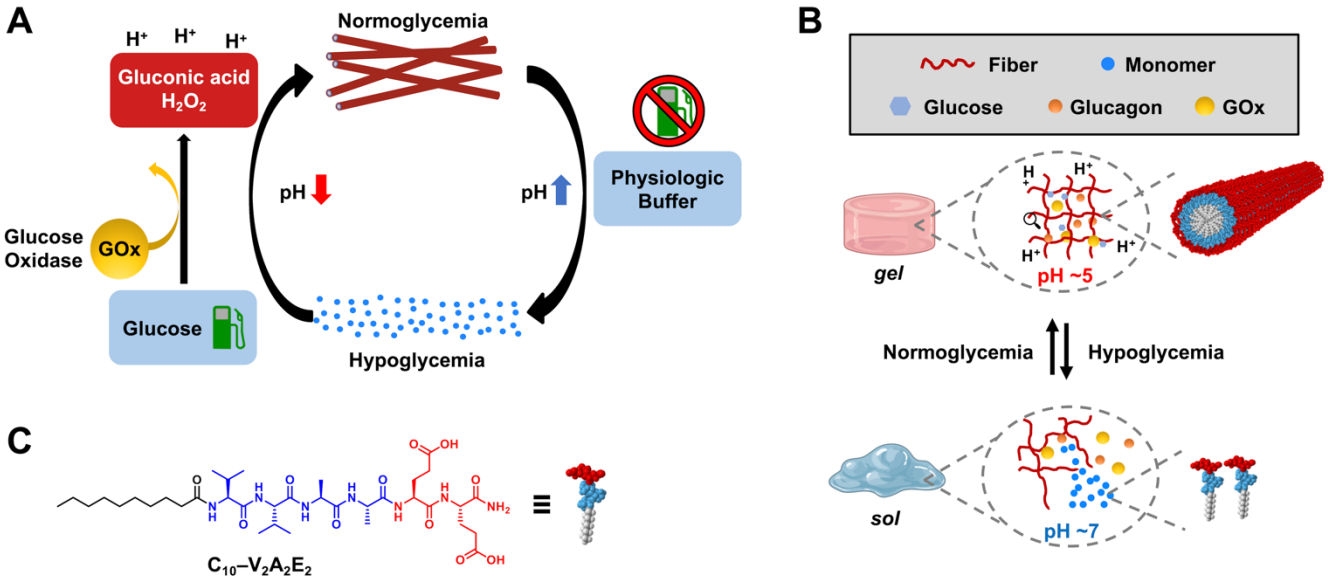

Figure 1: (A) Schematic of the cyclic process using glucose oxidase as an actuator to convert glucose fuel to a pH stimulus directing and stabilizing peptide assemblies. In conditions of limited glucose, natural physiological buffering restores the material to its destabilized state. **(B)** Materials stabilized in the presence of a glucose fuel reverses the traditional paradigm in glucose-responsive materials, instead targeting material stability in states of normal glucose and dissolution in low glucose to release a glucagon therapeutic. **(C)** Structure of the $C_{10}–V_2A_2E_2$ peptide amphiphile used in this work to achieve self-assembly and hydrogelation under direction of a glucose fuel.

responsive strategies for glucagon delivery may afford enhanced precision in insulin-centered blood glucose control while mitigating the severe risks of hypoglycemia.[11]

The construction of biomaterials and drug delivery devices from supramolecular interactions offers routes to endow stimuli-responsivity using tunable non-covalent associations.[12–14] In the field of supramolecular materials, non-equilibrium systems that form transiently by input of energy or consumption of chemical fuels constitute an exciting and growing body of research.[15,16] Enzymes are useful components of many non-equilibrium and/or fueled systems reported so far due to their ability to chemically transform a pre-assembled molecule or promote an environment favoring its (transient) assembly.[17–20] The use of disease-relevant enzymes or their substrates to facilitate transformations in supramolecular materials offers a possible strategy for improved therapeutic precision in drug delivery.[21,22]

In the context of glucose-responsive materials, glucose oxidase (GOx) has been commonly used to actuate glucose levels into a material-directing stimulus.[4] GOx catalyzes the conversion of one molecule of D-glucose into glucono-δ-lactone and H_2O_2, with the former hydrolyzing to gluconic acid.[23] Glucose-responsive hydrogels that incorporate GOx sensing use the reduction in microenvironmental pH from gluconic acid production to drive swelling or bond rupture in a polymeric network.[24–26] GOx has also been used to regulate gelation in pH-sensitive peptide gelators.[27,28] Here we present a nanofibrillar assembly that leverages GOx to drive non-equilibrium network formation of a peptide hydrogelator through the localized reduction in pH achieved by consumption of physiologic glucose "fuel" (***Fig 1***). In the absence of sufficient glucose fuel, as upon onset of hypoglycemia, a neutral-buffered physiological milieu acts as a directive to promote gel dissolution through molecular disassembly, restoring the equilibrium state. This approach contrasts with the preponderance of literature in glucose-responsive materials design that seeks to use glucose to drive material disassembly or erosion for the release of insulin, here instead offering a route to transiently stabilize nanofibrillar hydrogels in the presence of glucose. Accordingly, the present strategy is explored using glucose-stabilized materials for glucose-responsive delivery of glucagon as a preventative route to combat the subsequent onset of hypoglycemia.

RESULTS & DISCUSSION

Peptide Design. Peptides constitute a class of molecules extensively explored as supramolecular materials for biomedical applications.[29,30] To prepare a pH-responsive gelator and achieve self-assembly governed by consumption of glucose fuel (***Fig 1A-B***), the peptide amphiphile (PA) platform was explored here.[31] This supramolecular motif typically combines a hydrophobic directive for assembly in water from a saturated alkyl chain appended at a terminal position

with a peptide sequence consisting of residues for lateral association through β-sheet hydrogen bonding as well as residues bearing charged groups to enhance solubility and amphiphilicity of the molecule.[32] These molecules can self-assemble in water to form high aspect-ratio nanofibrils templated by hydrogen bonding along the long axis of the fiber, and further physically entangle to form percolated hydrogel networks. The interplay of attractive and repulsive forces entailed in this molecular design gives rise to a tunable extent of molecular cohesion,[33,34] and can be varied by altering tail length,[35] β-sheet sequence,[36] or the number/identity of charged residues. In particular, the electrostatic repulsion between charge-bearing hydrophilic amino acids can be modulated by addition of counterions or by changing pH relative to the pKa of charged residues so as to induce self-assembly, stabilize nanofibrils, and increase the extent of physical crosslinking in a resulting hydrogel.[37]

To interface a supramolecular PA gelator with glucose-fueled assembly directed by the enzymatic actuation of GOx, a variant was desired to form stable hydrogels in the acidic microenvironment that would result locally from conversion of a normal level of glucose, but which transitioned to a *sol* under glucose-limited conditions. GOx conversion of physiological levels of glucose to yield gluconic acid can lead to a microenvironmental pH in the range of ~4-5.[6] Accordingly, a molecular design was envisioned bearing the typical saturated alkyl chain and β-sheet-forming sequence coupled to glutamic acid as the hydrophilic domain; the pKa of its carboxylate R-group (~4.5) can shift upward in the range of 4.5-6 due to aggregation effects from PA self-assembly.[38] Accordingly, glutamic acid (E) should be significantly protonated (uncharged) at acidic pH levels achieved by GOx in normal glucose levels, yet deprotonated (negatively charged) at physiological pH. Different PA sequences were synthesized to vary the alkyl tail length (C_{10} and C_{16}) and valine(V)–alanine(A) β-sheet sequence (V_2A_2, VA_3, A_2V_2) with a conserved hydrophilic head group (E_2). The intention of screening this small set of molecules was to probe pH-responsive release to determine the optimal balance of attractive and repulsive forces required for the envisioned application of assembly at normal glucose (*i.e.,* low pH actuated by GOx) but disassembly and glucagon release in low glucose conditions (*i.e.,* neutral-buffered physiological pH). Based on a preliminary screen comparing release rates of a model macromolecule at pH 5 and 7 (***Fig S1***), a final sequence of C_{10}–$V_2A_2E_2$ (***Fig 1C***) was selected for further evaluation. The selected sequence has a shorter C_{10} alkyl segment than commonly used in most reported PA materials. The V_2A_2 sequence is thought to be effective for β-sheet hydrogen bonding,[39] while still being shorter than most commonly explored sequences.[36] The glutamic acid residues then afford pH sensitivity over the range desirable for GOx. Thus, a reduction in cohesive forces from a shorter alkyl segment and a 4-residue β-sheet forming segment was thought to enable more rapid responsiveness dependent on the charge state of the glutamic acid residues.

pH-Dependent Self-Assembly & Hydrogelation. Given the importance of pH to the envisioned mechanism of glucose-fueled assembly, pH-responsive self-assembly of lead PA C_{10}–$V_2A_2E_2$ was first characterized. Samples were prepared in buffers of pH values ranging from 5 to 8, cast as dry films, and imaged with transmission electron microscopy (TEM) (***Fig 2A***). It is noted that TEM performed on dry films is subject to artifacts arising from drying and sample concentration on the grid. However, qualitative observations support a general trend for a reduction in nanofibril length as well as reduced nanofibril bundling as pH was increased from 5 to 8. For example, samples at pH 5 had a high density of elongated nanofibrils with substantial bundling, while samples prepared at pH 8 had sparse nanostructure with observed nanofibrils being significantly shorter and exhibiting almost no bundling.

Near ultraviolet circular dichroism (CD) spectroscopy was performed to characterize amino acid secondary structure in buffers of various pH (***Fig 2B***). CD is frequently used to qualitatively assess the extent of β-sheet hydrogen bonding in PA materials. Spectra collected for C_{10}–$V_2A_2E_2$ at pH 5 exhibited a characteristic β-sheet signature with a negative peak at 220 nm and positive peak at 194 nm. Meanwhile, the CD spectra for the sample prepared at pH 8 exhibited a negative peak at 197 nm characteristic of a random coil secondary structure. The samples prepared at intermediate pH values of 6 and 7 were primarily random coil, with some evidence of residual β-sheet character for the pH 6 sample. These findings support increased β-sheet cohesion in self-assembled nanofibrils resulting from less electrostatic repulsion in the glutamic acid head group at lower pH. Fourier-Transform Infrared Reflectance (FTIR) spectroscopy was also performed to monitor signals attributed to β-sheet and random coil structures as a function of pH, revealing the same trend of β-sheet reduction and random coil emergence as pH increases (***Fig S2***).[40,41]

Thioflavin-T (ThT) provides another method to study the β-sheet character of peptide self-assemblies, relying on increased fluorescence of this dye when embedded in β-sheet-rich domains.[42] The background-subtracted fluorescence of C_{10}–$V_2A_2E_2$ at pH 5 and pH 7 was first compared; pH 5 exhibited strong ThT fluorescence indicative of ThT bound to β-sheet-rich structures while limited fluorescence was measured at pH 7 (***Fig 2C***). After 300 s incubation, the pH was increased to pH 7 rapidly by

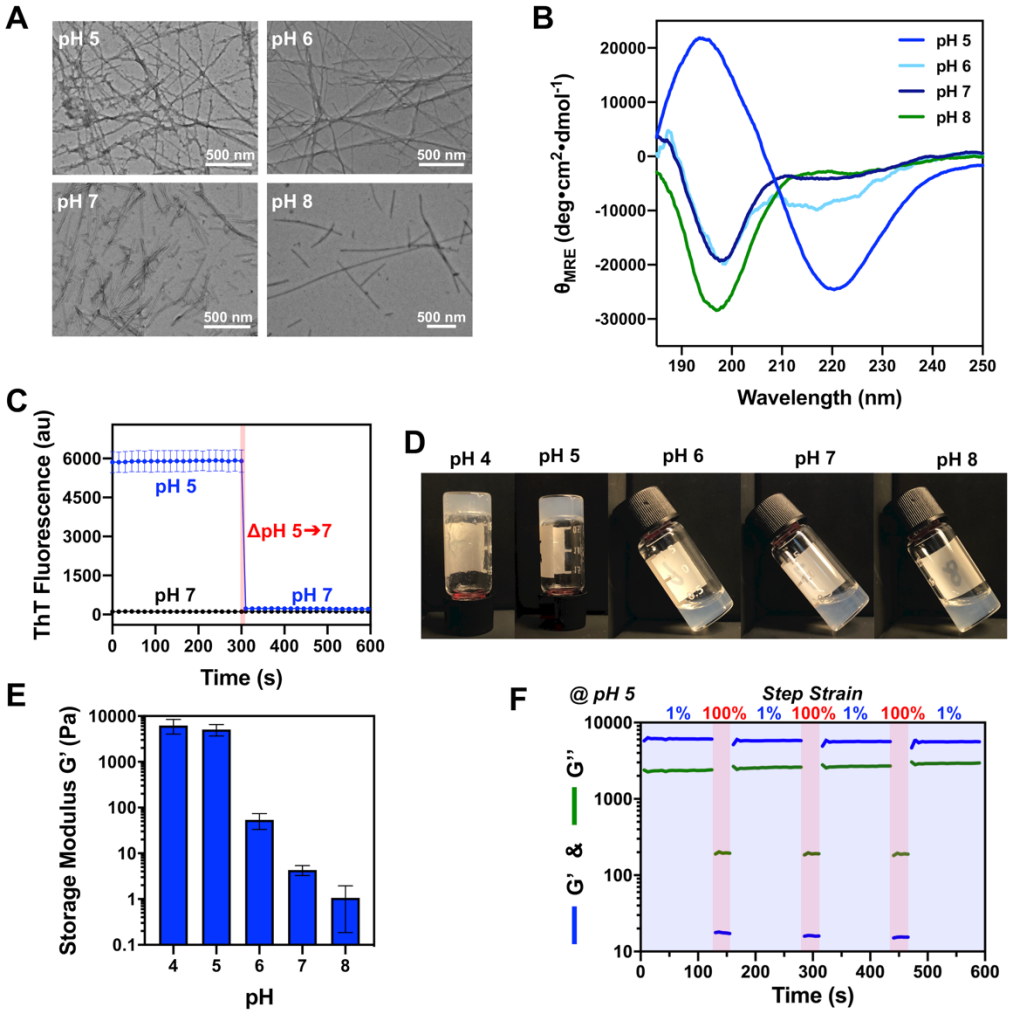

Figure 2: (A) Transmission electron microscopy to assess pH-dependent nanostructure formation of C_{10}–$V_2A_2E_2$ PA in films cast from 0.1% w/v PA solutions at various pH. **(B)** Near-UV circular dichroism spectroscopy of C_{10}–$V_2A_2E_2$ PA at various pH at a sub-gelation concentration of 0.1% w/v. **(C)** Background-subtracted thioflavin-T (ThT) fluorescence, comparing C_{10}–$V_2A_2E_2$ PA (0.1% w/v) when changed rapidly from pH 5 to pH 7 to a sample maintained at pH 7 throughout. **(D)** pH-directed hydrogel formation at 1% w/v C_{10}–$V_2A_2E_2$ PA in physiologic buffers of assorted pH. Images collected 15 min following sample preparation. **(E)** Plateau modulus for C_{10}–$V_2A_2E_2$ PA samples prepared at 1% w/v in a buffer of various pH (1% strain, 10 rad/s, average of 2 gels/group). **(F)** Step-strain rheological testing of C_{10}–$V_2A_2E_2$ PA hydrogels prepared at pH 5 and cycled at a frequency of 10 rad/s between 1% and 100% strain.

adding a small volume of NaOH. ThT fluorescence disappeared by the next reading (~15 s), indicating immediate loss of β-sheet character upon pH neutralization. Accordingly, pH offers an effective and rapid means to activate and deactivate stabilizing β-sheet structures in C_{10}–$V_2A_2E_2$ assemblies.

The gelation of C_{10}–$V_2A_2E_2$ was next studied at 1% w/v in buffers of pH 4 to pH 8 under physiologic salt concentration. Gross visual inspection of PA samples following equilibration at these various pH levels (*Fig 2D*) revealed the formation of a stable hydrogel immediately at pH 4 and pH 5. This observation aligns with the predicted pKa of the glutamic acid side-chain. At pH 6, the solution was notably viscous, yet this sample flowed when subjected to vial inversion. Samples prepared at pH 7 and pH 8 were even less viscous and flowed with relative ease upon vial inversion. It is noted that samples of all pH conditions were viscous and not fully translucent, indicating the presence of some nanostructure in all samples.

Vial inversion affords a crude means to inspect bulk differences in apparent hydrogelation. By contrast, rheological testing enables quantitative insights into the mechanical and dynamic properties of these materials.[43] Oscillatory rheology was thus performed to quantify the observed pH-dependent differences in hydrogelation. Samples were first assessed with a strain sweep to determine the linear viscoelastic range, and then gel-forming samples were subjected to a frequency sweep to verify the range of oscillatory frequency rates wherein the

storage modulus (G′) exceeded the viscous/loss modulus (G′′). As an example, a sample that formed a mechanically robust hydrogel in buffer at pH 5 exhibited linear behavior with G′>G′′ when exposed to strains in the range of ~0.1-5%, with the hydrogel being mechanically compromised at a critical strain of ~55% (***Fig S3***). This sample also exhibited scarce frequency-dependent G′ behavior, with G′ values ~10x higher than G′′ over the full range of frequency assessed. This behavior in a frequency sweep is indicative of relaxation times for physical interactions in the hydrogel network, such as nanofiber bundling and intersection, being significantly slower than the range of frequencies probed in dynamic rheological testing.

The G′ values for samples at each pH were compared at a constant strain of 1% and frequency of 10 rad/s. When comparing G′ values across the full range of pH explored (n=2 gels/sample), pH-dependent mechanical properties were clearly evident (***Fig 2E, Fig S4***). G′ values were found to decrease with increasing pH as follows: 6.2 kPa (pH 4), 5.1 kPa (pH 5), 53.7 Pa (pH 6), 4.3 Pa (pH 7), and 1.2 Pa (pH 8). Limited differences were observed for G′ in samples of pH 4 and pH 5, yet G′ was reduced by two orders of magnitude for samples prepared at pH 6 and another order of magnitude for samples prepared at pH 7. Samples prepared at pH 8 had G′ measurements at the lower limit of instrument sensitivity.

For peptide-based gelators, the magnitude of G′ is correlated with an increase in the length, stiffness, and extent of bundling for high aspect-ratio nanostructures in the hydrogel. An increased propensity for β-sheet hydrogen bonding often underlies these changes in stiffness.[36] Rheological data coupled with evidence from TEM, CD, FTIR, and ThT studies suggests a mechanism whereby the increased negative charge of assemblies at pH levels of 6 and above drives an increase in repulsive forces within nanofibers to reduce packing and β-sheet formation, shorten the overall nanofiber length, and promote lower extents of aggregation. For any structures that do form, electrostatic repulsion between nanofibers due to increased negative charges would act to limit the extent of fiber bundling and physical crosslinking. Accordingly, from these comparative rheological results, along with evidence from TEM, CD, FTIR, and ThT, it can be inferred that glutamic acid residues in the assembled structures have a likely pKa in the range of 5-6, thus leading to the dramatic shift in pH-dependent G′ observed when transitioning between these two pH levels.

Rheological testing under cyclic strain is typically performed to assess the self-healing capacity of a physically crosslinked hydrogel in the context of its suitability for injection-based applications.[44,45] Here, the PA hydrogel prepared at pH 5 was subjected to step-strain cycling between 1% and 100% strain at a constant frequency of 10 rad/s (***Fig 2F***). This high strain was selected to be in excess of the critical strain for the material (G′′>G′ at >55% strain). After multiple cycles of 30 s duration at high strain, G′ values for the material were recovered instantly upon a return to low strain. In the context of the eventual envisioned application of these materials, a stable hydrogel containing GOx could be administered in a pH 5 buffer through a syringe into a normoglycemic environment and recover its mechanical properties nearly instantly *in situ* prior to being placed under assembly control by consumption of physiological glucose fuel (***Movie S1***). Divalent cations like Ca^{2+} and Mg^{2+} are known to stiffen PA hydrogels of this type *via* ionic crosslinking of glutamic acids.[37] To assess whether such an effect would compromise pH-responsive properties *in vivo* by stabilizing nanofibers at neutral pH, CD and rheology were performed under physiological Ca^{2+} and Mg^{2+} levels. No change in the β-sheet content or storage modulus of the material was found at pH 7.4 upon introduction of these divalent ions (***Fig S5***).

Glucose-dependent Gelation. After pH-dependent self-assembly and gelation was established, glucose-dependent gelation was explored through the inclusion of GOx to actuate glucose into a pH stimulus. One benefit of hydrogelation of this material at 1% w/v is the significant hydrated and interconnected porosity (***Fig S6***) to enable encapsulation of proteins like GOx to drive gelation in response to glucose. Samples of C_{10}–$V_2A_2E_2$ were prepared at 1% w/v in buffer at pH 7.4, with glucose added to achieve concentrations ranging from 0 to 200 mg/dL (0 to 11.1 mM). These ranges of glucose were selected to span typical physiological glucose levels in the healthy state and extend down to levels corresponding to hypoglycemia. Following equilibration for 24 h, samples were assessed grossly for gelation by vial inversion (***Fig 3A***), as performed in pH-dependent gelation studies. Visual inspection following vial inversion revealed self-supporting hydrogels at glucose concentrations of 200 mg/dL and 150 mg/dL. The material prepared with 100 mg/dL glucose was very viscous but slowly flowed upon inversion, while those prepared at 0 mg/dL and 50 mg/dL were not self-supported on inversion.

Rheological studies were performed to quantify differences in hydrogel character arising from glucose (***Fig 3B***). Measurements were collected as before for gels prepared in each of the different glucose-containing buffers. The value of G′ increased with increasing levels of glucose, as follows: 10.2 Pa (0 mg/dL), 19.0 Pa (50 mg/dL), 29.5 Pa (100 mg/dL), 206.6 Pa (150 mg/dL), and 2.4 kPa (200 mg/dL). Given results of pH-dependent gelation for C_{10}–$V_2A_2E_2$ PA, it was expected that inclusion of GOx would actuate increased glucose level into a local

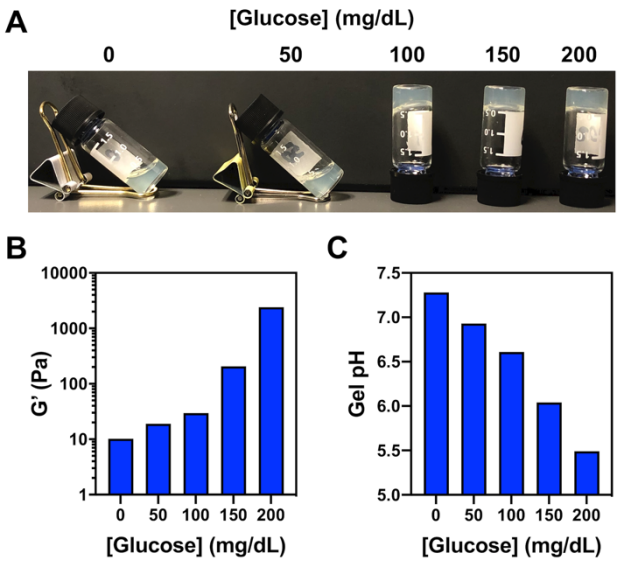

Figure 3: (A) Glucose-directed hydrogel formation at 1% w/v C_{10}–$V_2A_2E_2$ PA with GOx in physiologic buffers at pH 7.4 and with assorted glucose concentrations. Images collected 24 h following sample preparation. **(B)** Plateau modulus for C_{10}–$V_2A_2E_2$ PA samples prepared at 1% w/v in pH 7.4 buffer of various glucose concentrations (1% strain, 10 rad/s). **(C)** pH recorded by submersion of an electrode into hydrogel samples 24 h after under conditions of various glucose input.

reduction in pH driving hydrogelation. A microelectrode pH probe was submerged within each hydrogel (*Fig 3C*), and glucose-dependent pH reduction was recorded, ranging from pH 7.3 (0 mg/dL) to pH 5.5 (200 mg/dL). It is noted that all samples began at pH 7.4; enzymatic conversion of glucose afforded by GOx was thus responsible for reducing pH of the fluid within the hydrogel. These measured pH values support findings from rheology as higher G′ was observed at higher glucose concentration which translated to a lower sampled pH. In addition, these findings also confirmed results for the relationship between G′ and pH, with similar results obtained for comparable pH values realized upon addition of glucose. Small discrepancies in G′ values between the pH and glucose studies presented here may be attributed to inclusion of the large GOx protein (160 kDa) within the nanofibrillar mesh of the hydrogel. The fixed and finite glucose concentrations within these small volume hydrogels may somewhat limit direct comparisons with concentrations for their use in a physiological setting, as a replenishable glucose supply could further stiffen the materials through enhanced pH reduction.

The results of these glucose-dependent gelation studies support this platform coupled with GOx to translate glucose levels into changes in nanoscale and bulk material properties. Based on common interpretations of G′ values for nanofibrillar peptide hydrogels, higher glucose concentrations here corresponded to a more highly interconnected network arising from physical interactions between longer and stiffer nanostructures. As glucose levels were reduced to approach hypoglycemic levels, the network topology as measured by G′ decreased by several orders of magnitude. Thus, the self-assembly of C_{10}–$V_2A_2E_2$ PA coupled with GOx afforded a reliable platform wherein local glucose concentration could be manifest in hydrogel formation and mechanical properties.

Glucose-Dependent Glucagon Release. After identifying a gelator capable of both pH- and glucose-responsive self-assembly and hydrogelation, controlled release of an encapsulated therapeutic glucagon payload was next assessed. Screening of PA sequences had identified the lead sequence on the basis of pH-dependent controlled release of a neutral model macromolecule (3kDa FITC-dextran, *Fig S1*), supporting a mechanism of pH-directed change in network structure dictating the rate of passive release of macromolecules comparable in size to glucagon. For functional release studies, the dasiglucagon analogue was selected as the payload due to its improved solubility and stabilized secondary structure relative to native glucagon.[46] For ease in detection during release studies, a fluorescent methoxycoumarin (MCA) group was substituted in place of a tryptophan on the dasiglucagon sequence. Hydrogels were prepared in all cases in a pH 5 buffer at 1 % w/v to ensure initial gelation. Each 100 µL hydrogel also contained GOx, catalase, and 0.2 mg of MCA-dasiglucagon. It is noted that catalase was added to these formulations in order to catalyze the conversion of the toxic GOx byproduct, H_2O_2, into H_2O and O_2 in advance of *in vivo* application, as is commonly done to reduce toxicity for other GOx-based glucose-responsive materials.[47] Each hydrogel was immersed in 4 mL pH 7.4 buffer containing different physiologically relevant glucose concentrations, while a control hydrogel was immersed in a pH 5 buffer to understand dasiglucagon leakage from the fully stable hydrogel. In order to maintain desired glucose concentrations for each group, a small volume of a concentrated glucose solution was added during release studies to replenish the glucose fuel consumed by GOx, enabling stable glucose concentrations over time as confirmed by glucometer readings.

Studying release over a range of glucose concentrations revealed clear glucose-dependent dasiglucagon release (*Fig 4A*), with both the rate and amount of dasiglucagon release decreasing with increasing glucose levels in the buffer. At 24 h, retained dasiglucagon in each sample was extracted and quantified to verify mass balance closure (*Fig 4B*). When time-dependent release data were fit to a standard first-

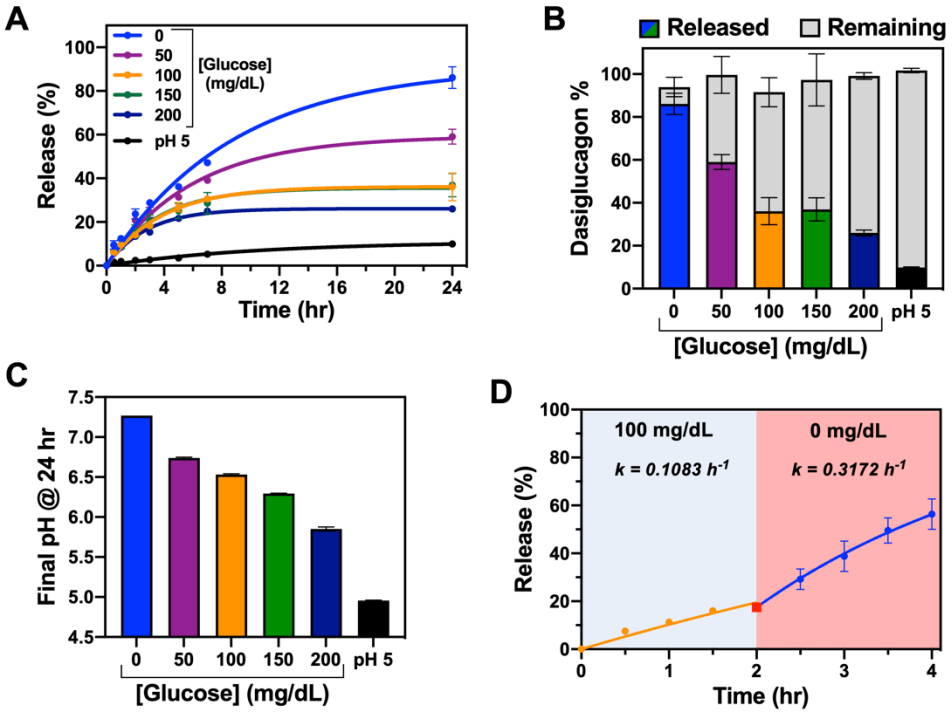

Figure 4: (A) Glucose-dependent release of MCA-dasiglucagon from within 100 µL of 1% w/v C_{10}–$V_2A_2E_2$ PA hydrogels with GOx prepared initially in pH 5 buffer and then incubated in a bulk solution of 4 mL pH 7.5 buffer containing different levels of dissolved glucose. Data were fit to a standard first-order release model. **(B)** Total MCA-dasiglucagon released at 24 h, combined with MCA-dasiglucagon remaining within residual material after treatment of the system with concentrated base (gray bars in all cases). **(C)** Final pH of the release system after 24 h. **(D)** Step-change release, beginning with hydrogels prepared at 100 mg/dL glucose and then exchanging the full 4 mL release buffer with a buffer containing 0 mg/dL glucose at 2 h (red point).

order model, the model plateau values obtained ranged from 91% (0 mg/dL) to 26% (200 mg/dL), indicating the role of GOx conversion of glucose in stabilizing the hydrogel and limiting its release of encapsulated dasiglucagon. The pH 5 control hydrogel, meanwhile, showed slow and limited release with a first-order plateau value of 11%. The inclusion of GOx was critical to achieving controlled dasiglucagon release in the presence of glucose (*Fig S7*). The pH of the bulk buffer, which began at pH 7.4, decreased at 24 h as a result of acidification from GOx action, reaching a pH of 5.9 in the buffer containing 200 mg/dL glucose (*Fig 4C*). This reduction in bulk pH occurred steadily over the first several hours of gel incubation (*Fig S8*). The initial release rates during the first 3 h of incubation were also higher for samples incubated in 0 mg/dL (12.3%/hr) compared to those in 200 mg/dL glucose (7.3%/hr), supporting glucose-dependent release even at early times before a significant bulk acidification was realized to stabilize the hydrogel and slow release. It is noted that bulk pH measurements do not necessarily reflect the local microenvironmental pH within the hydrogel that may arise from concentration gradients, preferential proton localization, and/or differential pH buffering by charged residues of the material. Local reductions in microenvironmental pH have been postulated as a mechanism for function of many related hydrogel systems that use GOx to induce pH-responsive swelling and insulin release.[24–26] The lag in glucose-induced material stabilization, and concomitant burst release in the initial period, offers an opportunity for future refinement of these and related technologies.

GOx activity was preserved within the gel for at least 10 d based on its ability to repeatedly lower pH upon daily recharge with an unbuffered and neutral 200 mg/dL glucose solution (*Fig S9*). This is expected given the weeks-long use of GOx as a sensor in implanted continuous glucose monitors.[48] Moreover, the dasiglucagon payload remains stable for at least 7 d of incubation in the pH 5 environment expected within the hydrogel, showing no sign of degradation or amyloid formation (*Fig S10*).

The envisioned application for glucagon delivery using glucose-stabilized materials is as an administered prophylactic, ready in the event of subsequent onset of a serious hypoglycemic episode. Thus, a rapid reduction in glucose level should trigger material dissipation and accelerated glucagon release. To assess this use, hydrogels prepared identically to those in the release

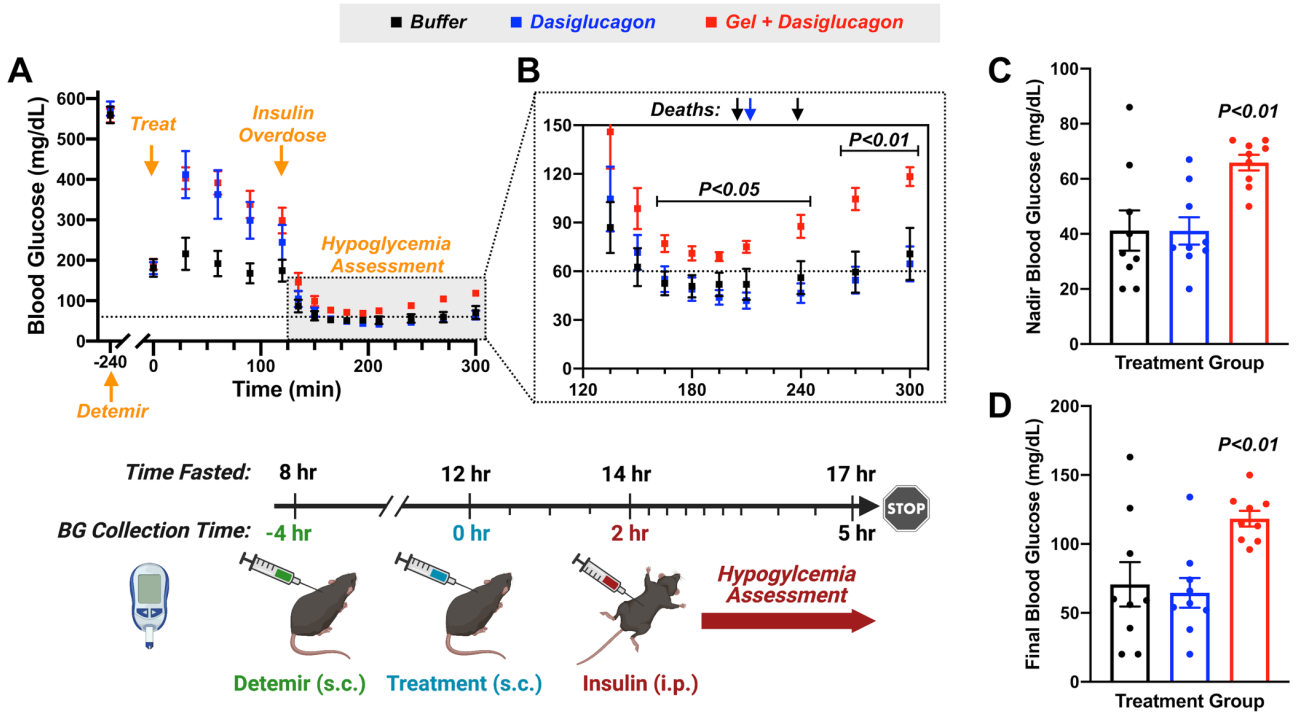

Figure 5: (A) A cartoon schematic overview with data for the full *in vivo* experimental model to assess prophylactic hypoglycemia correction with C_{10}–$V_2A_2E_2$ PA hydrogels. STZ diabetic mice were fasted and then administered *insulin detemir* to stabilize blood glucose within a normal range. After 4 h, treatments were then administered (t = 0) and blood glucose was monitored. At 2 h after treating with buffer, dasiglucagon, or PA hydrogel, an insulin overdose was performed. Blood glucose was monitored throughout the study. A dashed line is drawn at 60 mg/dL for visualization of the approximate region characterized clinically as mild hypoglycemia (*<70 mg/dL but >54 mg/dL*). **(B)** The extent and duration of hypoglycemia was evaluated between treatments with arrows noting the timing of observed deaths. **(C)** The nadir (lowest) blood glucose reading, as well as **(D)** the final blood glucose measured at 300 min was also compared between groups. Each treatment group was n=9 mice, error bars indicate SEM for each group, and statistical analysis was performed using ANOVA with multiple comparisons post-hoc testing.

studies were first incubated in a buffer of 100 mg/dL (resembling normoglycemia) and following 2 h the buffer was exchanged to 0 mg/dL (*Fig 4D*). The instantaneous reduction in glucose led to an acceleration in dasiglucagon release from 10.8%/hr before the buffer change to 31.7%/hr after. In this case, release when the sample was switched to 0 mg/dL glucose was even faster than it was in the case where the experiment was initialized from 0 mg/dL glucose buffer. Complete buffer exchange can increase release due to dilution, swelling, and/or gel erosion, but this alone did not account for the more rapid release following introduction of the glucose-free buffer (*Fig S11*).

Hypoglycemia Prevention in Diabetic Mice. With a hydrogel material that leveraged GOx to achieve stability in the presence of a consumable glucose fuel but which dissipated under conditions of reduced glucose to accelerate the release of its dasiglucagon payload, the next step was to assess the protective effect of this material to limit the onset and severity of a subsequent hypoglycemic event. For these studies, a mouse model was developed using streptozotocin (STZ) for chemically induced diabetes. STZ mice were chosen due to reports of dose-dependent increase in insulin secretion and blood glucose *reduction* seen for healthy mice treated with glucagon.[49] Following onset of severe diabetes, the hydrogel technology reported here was assessed in a prophylactic capacity to limit the onset and severity of hypoglycemia upon an insulin overdose (*Fig 5*).

With limited reports assessing the protective use of glucose-responsive glucagon therapy, it was necessary to develop an animal model that could recreate some of the clinical features expected in using a material designed to maintain sequestered glucagon onboard in the event of a subsequent hypoglycemic episode (*Fig 5A*). STZ mice were fasted to increase sensitivity to both insulin and glucagon and limit confounding data arising from variable eating patterns. After a 9 h fast, basal *insulin detemir* (Novo Nordisk, *Levemir*®) was administered to correct blood glucose to within the normoglycemic range for a healthy mouse (~180-200 mg/dL) to simulate insulin-dependent blood glucose control in diabetes. *Insulin detemir* is a clinically used derivative that leverages serum albumin binding through its modification with a

saturated alkyl chain to achieve long-lasting basal function, offering a duration of action of ~18-20 h in humans.[50] The intention of this step was to achieve a consistent blood glucose level in mice on a plane of normoglycemia, an outcome evident in data for all mice reported in this study (184 ±49 mg/dL, mean ±std dev, n=27). Treatments (n=9/group) consisting of a sham (buffer) control, a dose of 0.01 mg dasiglucagon, or 1 % w/v hydrogel containing 0.01 mg dasiglucagon along with GOx/catalase were next administered subcutaneously. Following 2 h, an insulin challenge was performed by injection of recombinant human insulin to induce hypoglycemia. Blood glucose was monitored serially throughout the process.

Following treatment with dasiglucagon alone or loaded within the hydrogel, blood glucose level sharply increased relative to the buffer control at 30 min (***Fig 5A***). This finding indicates active signaling of dasiglucagon in both treatments. Such a rapid peak is consistent with the known time to action of dasiglucagon in clinical trials.[46] Unfortunately, this result points to leakage of active dasiglucagon upon administration of hydrogels under normoglycemic conditions; this is to be expected based on the near-instant release of ~20% of the dasiglucagon payload for release assays at 200 mg/dL. Future iterations of glucose-fueled hydrogels for dasiglucagon delivery, particularly if intended as prophylactic rescue devices, must address this initial burst release so as not to interfere with the process of blood glucose control in insulin-centered therapeutic management.

Hypoglycemia was induced 2 h after prophylactic glucagon treatment by intraperitoneal administration of recombinant insulin and blood glucose was monitored to track the onset and severity of hypoglycemia (***Fig 5B, Fig S12***). The average blood glucose for mice treated with dasiglucagon-loaded hydrogels exceeded that for the other two treatments, achieving significantly ($p<0.05$) higher blood glucose at 45 min following insulin challenge through the end of the study. The extent of hypoglycemia can be visualized by the minimum (nadir) blood glucose value measured for each group (***Fig 5C***). By this metric, the nanofibrillar hydrogel treatment (65.9 ±2.8 mg/dL) demonstrated significantly ($p<0.01$) less hypoglycemia than treatment with either dasiglucagon alone (41.1 ±5.0 mg/dL) or the buffer control (41.2 ±7.3 mg/dL). Not only did the nanofibrillar hydrogel delivery limit the onset and extent of hypoglycemia, but it demonstrated protection compared to limited observations of death for buffer (2 of 9) and dasiglucagon (1 of 9) treatments (***Fig 5B***).

To assess recovery from hypoglycemia, blood glucose levels were compared at the endpoint of the study, 3 h following insulin challenge and 5 h following administration of prophylactic treatment. By this metric, the nanofibrillar hydrogel treatment (118.3 ±5.7 mg/dL) demonstrated significantly ($p<0.01$) faster recovery than treatment with either dasiglucagon alone (65.6 ±10.8 mg/dL) or the buffer control (70.7 ±16.1 mg/dL) (***Fig 5D***). Taken together with data showing a reduced severity of hypoglycemia, these data demonstrate that the nanofibrillar hydrogel achieves more rapid recovery following induction of hypoglycemia.

The fully formulated 50 µL hydrogel was located through necropsy in the subcutaneous space for up to 5 d following its administration in healthy mice, but could not be located at 7 d. As such, the material has reasonable stability over multiple days following administration, even when applied to a healthy mouse at a normoglycemic state. Yet the stability over time under normoglycemic conditions still lags behind related PA-based materials that form stable hydrogels at neutral pH, which remain in the subcutaneous tissue for over 30 d.[51] Preliminary experiments also supported a functional role for GOx in actuating blood glucose level to dictate dasiglucagon release from the hydrogel *in vivo*, supporting glucose-dictated release as opposed to simple controlled release as the mechanism of hydrogel function in protecting against hypoglycemia (***Fig S13***).

The limited prior studies evaluating glucagon release triggered by insulin overdose and hypoglycemia makes contextualizing the present findings a challenge. Microneedle arrays have been most commonly explored in this area, leveraging insulin-binding aptamers or glucose-binding phenylboronic acid polymers to trigger transcutaneous release of encapsulated glucagon.[11,52,53] Compared to these works, the current model may be more clinically relevant in its use of basal insulin *insulin detemir* to begin studies from a point of glucose control instead of from a hyperglycemic (*e.g.*, 400+ mg/dL) state. The use of fasting, and the protocols in cases where it has been previously used, also vary across these prior studies. Nonetheless, the results presented here compare favorably. In terms of protection against hypoglycemia, 0 of 9 mice treated with the glucagon-loaded nanofibrillar hydrogel reached levels below 50 mg/dL, whereas 7 of 9 mice in the buffer-treated group fell below this same level. This extent of hypoglycemia in the control is at least as severe as that reported in other studies,[53] validating the relevance of the present model. Compared to this same prior work, the glucagon-treated group here began to recover from hypoglycemia within 90 min of insulin challenge, whereas the blood glucose profile in these prior glucagon-releasing microneedles remained flat or slightly decreased for the full period shown following insulin overdose (2.5 h).[53] The expected duration of action for *insulin detemir* in the present model also means that recovery occurs in spite of residual basal insulin action.

Overall, the results presented here to use transient glucose-stabilized hydrogels for glucagon delivery demonstrate promise in the context of other works in this space.

Glucagon leakage leading to blood glucose instability under conditions of normoglycemia would not be ideal for a once-nightly prophylactic treatment to prevent sudden onset of nocturnal hypoglycemia, as in the envisioned use case here. At the same time, glucagon has been actively explored in affording better control and more effective insulin dosing, such as in clinical work exploring control from dual-hormone pumps.[54] Thus, technologies like the current system that offer glucose-directed control over the rate of glucagon release may be integrated more broadly within an arsenal of therapeutic strategies for better and more responsive blood glucose management, working to deliver on approaches seeking a "fully synthetic pancreas."[7] Indeed, inspirational work in dual-hormone microneedles points to a possibility for future material designs that pair on-demand glucagon and insulin release for better blood glucose control.[11]

CONCLUSIONS

The approach outlined here demonstrates the use of enzymatic actuation consuming a ubiquitous biological and disease-relevant glucose fuel to drive the formation and stability of a supramolecular nanofibrillar hydrogel. These materials afforded glucose-directed release of a therapeutic glucagon analogue in a manner inversely related to glucose concentrations, spanning a physiologically relevant range. Moreover, this approach demonstrated the capacity to limit both the extent and duration of hypoglycemia in a diabetic mouse model when administered in a prophylactic capacity in advance of an insulin challenge. Relative to the body of work in glucose-responsive materials, the majority of which respond to *high* glucose levels to release insulin, the present approach offers a new paradigm in material design. This observation of material stability in the presence of continuously available glucose fuel is furthermore reminiscent of work seeking to achieve non-equilibrium steady states in materials under enzymatic control.[18] With inspiration from many functional non-equilibrium materials in the living world, routes to engineer synthetic analogues of such materials have been active areas of discovery. Whereas the vast majority of such non-equilibrium systems reported to date are highly fundamental or have leveraged non-biologically relevant fuel sources, the present work demonstrates functional utility of similarly inspired approaches to engineer materials for a therapeutic application driven by a biological and disease-relevant glucose analyte as fuel. Accordingly, this general approach to develop glucose-fueled responsive materials holds promise for further development, either as a protective approach against hypoglycemia or as a component of a fully synthetic strategy for dual-hormone blood glucose control in diabetes.

EXPERIMENTAL METHODS

Peptide Synthesis & Purification. Peptide amphiphiles (e.g., C_{10}–$V_2A_2E_2$, **Fig 1C**) were synthesized by solid-phase methods using a CEM Liberty Blue automated synthesizer. Rink amide resin (0.89 emq/g, 100-200 mesh) and Fmoc-protected amino acids were purchased from ChemImpex. Fmoc removal was achieved using 20% piperidine in DMF, with couplings conducted under microwave heating using diisopropylcarbodiimide (DIC) and Oxyma in DMF. Peptides were cleaved from resin and protecting groups were removed by agitation in trifluoroacetic acid (TFA)/triisopropylsilane/H_2O (95:2.5:2.5, v/v/v) for 2 h at room temperature. The solution was evaporated under vacuum to remove most TFA and the product was recovered by precipitating in cold diethyl ether and collected by centrifugation. A solid white powder was air-dried overnight. Peptide purification was next performed on a Biotage Isolera system. The fully dried sample was dissolved in hexafluoro-2-propanol (HFIP) at a concentration of 100-150 mg/mL and injected onto a reversed-phase bio-C_{18} flash cartridge (50g) at a flow rate of 40 mL/min with the linear gradient from 0-100% (v/v) acetonitrile (+0.1% NH_4OH) in water. UV absorbance was monitored at 220 and 280 nm for fraction collection. The purified sample was collected and purity was verified by electrospray ionization mass spectrometry (ESI-MS, Advion, ***Fig S14***) and analytical HPLC on a C_{18} Gemini (Phenomenex) column (***Fig S15***). The purified fractions were lyophilized, yielding a white powder product.

The stable modified glucagon analogue, known as dasiglucagon (sequence reported[46]), and a fluorescent dasiglucagon variant modified with methoxycoumarin (MCA-dasiglucagon) were synthesized and purified according to similar methods as detailed above. To prepare a fluorescent MCA-dasiglucagon, MCA-lysine (Sigma) was inserted in place of the tryptophan residue at position 25. Both products were verified by ESI-MS and analytical HPLC (***Figs S16-S19***). The native conformation of dasiglucagon was verified by circular dichroism spectroscopy (***Fig S20***). The fluorescent properties of MCA-dasiglucagon was verified spectroscopically (***Fig S21***).

pH-dependent Self-assembly & Hydrogelation. The C_{10}–$V_2A_2E_2$ peptide amphiphile was first dissolved in DI water at a concentration of 2% (w/v). The solution was adjusted to pH 7.4 using 0.1 M HCl, and then mixed with

an equal volume of citrate-phosphate buffer (150 mM buffer +150 mM NaCl) at different pH (4, 5, 6, 7, 8) to form a gel at a concentration of 1% (w/v) in a final buffer concentration of 150 mM.

Glucose-dependent Self-assembly & Hydrogelation. The C_{10}–$V_2A_2E_2$ peptide amphiphile was first dissolved in DI water at a concentration of 2% (w/v). The solution was adjusted to pH 7.4 using 0.1 M HCl, and then mixed with an equal volume of 300 mM NaCl solution containing 440U/mL GOx and different glucose concentration (0, 100, 200, 300, 400mg/dL) to achieve final glucose concentrations of 0, 50, 100, 150, and 200mg/dL and final peptide concentration of 1% (w/v).

Rheological Characterization. Dynamic oscillatory rheology was performed on a TA Instruments Discovery HR-2 rheometer fitted with a Peltier stage using a parallel plate geometry with diameter of 25 mm to test the mechanical properties of all peptide hydrogels. Samples were prepared at a concentration of 1% (w/v) in buffers of different pH or glucose concentration, as described above, and measured 24 h after gel preparation. An amplitude sweep was first performed to determine the linear viscoelastic range for each hydrogel condition, and then a frequency sweep was performed at constant strain. Subsequently, a time-sweep (1% strain, 10 rad/s angular frequency) was performed for all hydrogels to measure and compare the storage modulus (G'). A step-strain study alternating between 1% strain for 2 min and 100% strain for 30 s at angular frequency 10 rad/s was also performed for the pH 5 hydrogel.

Circular Dichroism Spectroscopy. Near-UV circular dichroism spectroscopy (CD) was performed using a Jasco J-815 instrument. Samples were typically prepared at a concentration of 0.1% (w/v) in 50mM phosphate buffer at various pH (5-8) and 50 μL peptides solution was transferred to a quartz plate cuvette with pathlength of 0.1 mm. Three spectra were collected (range of 250-185 nm, 50 nm/min scanning speed) and averaged for each sample. For quality control, spectra were truncated upon photomultiplier voltage (HT) exceeding 600 mV.

FTIR. The peptide was first dissolved in D_2O at a concentration of 2% (w/v). The solution was adjusted to pH 7.4 using 0.1 M deuterium chloride (DCl), and then mixed with an equal volume of citrate-phosphate buffer prepared in D_2O (150 mM buffer +150 mM NaCl) at different pH (5, 6, 7, 8) to form a gel at a concentration of 1% (w/v) in a final buffer concentration of 150 mM. Gel samples of 10 μL for each pH were dropped, dried for 10 minutes, and analyzed using a Jasco FT/IR-6300 spectrometer. A background of the buffer in D_2O was subtracted from all spectra.

ThT Assay. Peptide solutions at concentration of 0.1% (w/v) were prepared in citrate-phosphate buffer (15mM buffer + 150mM NaCl) at pH value of 5 and 7 separately. Subsequently, 198 μL of these peptide solutions were combined with 2 μL of a 10 mM Tht stock. Fluorescence was measured on a Tecan M200 plate reader (Ex: 485 nm, Em: 528 nm) every 15 s. Following 300 s of equilibration, 2 μL 1M NaOH was added into pH 5 peptide solution reaching a final pH value of 7. For pH 7 peptide solution, 2 μL DI water was added. The volume of NaOH was verified to achieve pH 7 in this buffer system. The change of fluorescence intensity for both solutions was immediately recorded over another 300 s. A background of ThT in pH 5 and pH 7 buffer was subtracted from all spectra.

Transmission Electron Microscopy. Transmission electron microscopy (TEM) was performed using a JEOL 2011 instrument. Peptide samples were prepared at a concentration of 0.1% (w/v) in a 50mM phosphate buffer, at various pH (5, 6, 7, 8). These samples were deposited at a volume of 10μL onto a carbon-coated copper grid (200 mesh), wicked using filter paper after 30 s, and stained using 5 μL of a uranyl acetate solution. Grids were dried overnight prior to imaging.

Scanning Electron Microscopy. Peptide hydrogel samples were prepared at a concentration of 1% (w/v) in pH 5 citrate-phosphate buffer and fixed in a 4% glutaraldehyde solution in the same buffer at 4 °C overnight. Fixed peptide samples were washed in citrate phosphate buffer and DI water and serially dehydrated in 35%, 50%, 70%, 95%, and 100% ethanol. The dehydrated samples were dried using an Autosamdri®-931 CO_2 critical point dryer (Tousimis, Rockville, MD, USA). The dried samples were sputter-coated with a 3 nm Iridium layer and imaged using a FEI Magellan 400 field-emission scanning electron microscope at an accelerating voltage of 2 kV.

Glucose-dependent Glucagon Release. To evaluate glucose-responsive dasiglucagon release, 100 μL peptide hydrogels (1% w/v) containing 11 U GOx, 38.84 U catalase, and 0.02 mg MCA-dasiglucagon were prepared in pH 5 citrate-phosphate buffer. Once formed, the hydrogels were incubated within 6-well plates in 4 mL of either pH 5 or pH 7.4 buffer for pH-dependent release, or in a pH 7.4 buffer containing 0, 50 100, 150, 200 mg/dL glucose for glucose-dependent release. At each time point, a 20 μL aliquot was taken for fluorescence analysis (Ex: 322 nm, Em: 398 nm) with the MCA-dasiglucagon concentration determined using a standard curve (***Fig S21***). As glucose was continually consumed during the study, 20 μL of concentrated glucose solution was added to maintain a constant glucose level as verified by readings using a handheld glucometer. After 24 h, all samples were treated with 0.1 M NaOH to disrupt any remaining hydrogel structure and fluorescence of

residual MCA-dasiglucagon was measured to ensure mass balance closure. The pH of the bulk release buffer was also measured using a pH meter. To evaluate the impact of a sudden drop in glucose level on release, a 50 μL hydrogel containing 5.5 U GOx, 19.42 U Catalase, and 0.01 mg MCA-dasiglucagon was incubated in 2 mL pH 7.4 buffer containing 100 mg/dL glucose for 2 h. Subsequently, the incubation solution was removed and replaced with the same volume of pH 7.4 buffer containing no glucose.

Blood Glucose Control *in vivo*. To assess the ability of this technology to act in a preventative role to limit the onset and severity of hypoglycemia, a mouse model was established. Male C57BL6/J mice, aged 8 weeks, were induced to be diabetic by the destruction of pancreatic β-cells using a single intraperitoneal (i.p.) injection of streptozotocin (STZ, Cayman Chemical) at a dose of 150 mg/kg, according to published dosing protocols.[55] It is noted that for the dosing of all compounds and agents here, mice were assumed to have a body weight of 25 g. Insulin-deficient diabetes was verified at 9-13 d following STZ treatment using handheld blood glucose meters (CVS brand) to ensure unfasted blood glucose (BG) levels of 600+ mg/dL. These glucometers measure blood glucose values in the range of 20-600 mg/dL. For convention in presenting data, values of "high" are plotted as 600 mg/dL, while values of "low" are plotted as 20 mg/dL. Mice were fasted overnight for a period of 9 h, after which time BG was again measured. Mice having a fasted BG <450 mg/dL were triaged and removed from further study. Remaining mice were dosed with basal *insulin detemir* (*Levemir®*, *Novo Nordisk*) *via* subcutaneous (s.c.) injection at a dose of 0.5 IU/kg in a total injection volume of 100 μL. Following an additional 4 h fast to normalize blood glucose levels to a normal range for mice (~180 mg/dL), mice were randomized into groups and treated with buffer, dasiglucagon alone (0.01 mg), or the full PA hydrogel system at pH 5 and 1% w/v loaded with 0.01 mg dasiglucagon, 1.1 U GOx, 7.77 U Catalase in a 50 μL s.c. injection. This material formulation was verified to be stable following extrusion through a syringe into a pH 7 buffer containing 100 mg/dL glucose (***Movie S1***). Blood glucose was monitored serially following treatment, which for purposes of data visualization was set as t=0 min. At 2 h following administration of treatments, hypoglycemia was induced by i.p. injection of AOF recombinant human insulin (Gibco) at a dose of ~2.5 IU/kg in 100 μL of saline. BG levels were monitored for an additional 3 h after insulin overdose to monitor the onset of, and recovery from, hypoglycemia. Mice exhibiting "low" readings, as well as those which died from hypoglycemia, were noted with BG values of 20 mg/dL. In total n=9 mice per group were assessed by these methods, performing all treatments in two separate experiments on different mouse cohorts at different times and combining the data for analysis here. Mice were fasted for the duration of the study but had continuous access to water. These studies were detailed in a protocol approved by the University of Notre Dame Animal Care and Use Committee and adhered to all relevant Institutional, State, and Federal guidelines. Statistical testing between treatment and control groups was performed using one-way ANOVA with Tukey multiple comparison *post-hoc* testing (Graphpad Prism v9.0).

ASSOCIATED CONTENT

Supporting Information

The Supporting Information is available free of charge on the ACS Publications website.

Supplemental and supporting data sets: PA sequence screening, FTIR, supplemental rheology, SEM images, supplemental release studies, GOx function, dasiglucagon stability, supplemental *in vivo* data; molecular characterization: HPLC, ESI-MS, spectroscopy. (.PDF)

Movie of simulated injection (.MOV)

AUTHOR INFORMATION

Corresponding Author

* mwebber@nd.edu

Notes

The authors declare no competing financial interests.

ACKNOWLEDGMENT

MJW gratefully acknowledges funding support for this work from the Helmsley Charitable Trust (2019PG-T1D016), American Diabetes Association Pathway Accelerator Award (1-19-ACE-31), Juvenile Diabetes Research Foundation (5-CDA-2020-947-A-N), and National Science Foundation CAREER award (BMAT, 1944875). The authors are also grateful to Dr. Yuanhui Xiang and Guoqiang Liu for helpful conversations and insights into experimental design. Schematics in TOC artwork, Fig 1, and Fig 5 created using BioRender.com.

REFERENCES

(1) Mura, S.; Nicolas, J.; Couvreur, P. Stimuli-Responsive Nanocarriers for Drug Delivery. *Nat. Mater.* **2013**, *12* (11), 991–1003.

(2) Lu, Y.; Aimetti, A. A.; Langer, R.; Gu, Z. Bioresponsive Materials. *Nature Reviews Materials*. 2017. https://doi.org/10.1038/natrevmats.2016.75.

(3) Culver, H. R.; Clegg, J. R.; Peppas, N. A. Analyte-Responsive Hydrogels: Intelligent Materials for Biosensing and Drug Delivery. *Acc. Chem. Res.* **2018**, *51* (10), 2600.

(4) VandenBerg, M. A.; Webber, M. J. Biologically Inspired and Chemically Derived Methods for Glucose-Responsive Insulin Therapy. *Adv. Healthc. Mater.* **2019**, *8* (12), e1801466.

(5) Bakh, N. A.; Cortinas, A. B.; Weiss, M. A.; Langer, R. S.; Anderson, D. G.; Gu, Z.; Dutta, S.; Strano, M. S. Glucose-Responsive Insulin by Molecular

and Physical Design. *Nat. Chem.* **2017**, *9* (10), 937–943.
(6) Wang, J.; Wang, Z.; Yu, J.; Kahkoska, A. R.; Buse, J. B.; Gu, Z. Glucose-Responsive Insulin and Delivery Systems: Innovation and Translation. *Advanced Materials*. 2020, p 1902004. https://doi.org/10.1002/adma.201902004.
(7) Webber, M. J.; Anderson, D. G. Smart Approaches to Glucose-Responsive Drug Delivery. *J. Drug Target.* **2015**, *23* (7-8), 651–655.
(8) Leckie, A. M.; Graham, M. K.; Grant, J. B.; Ritchie, P. J.; Frier, B. M. Frequency, Severity, and Morbidity of Hypoglycemia Occurring in the Workplace in People with Insulin-Treated Diabetes. *Diabetes Care* **2005**, *28* (6), 1333–1338.
(9) Hsieh, A.; Twigg, S. M. The Enigma of the Dead-in-Bed Syndrome: Challenges in Predicting and Preventing This Devastating Complication of Type 1 Diabetes. *J. Diabetes Complications* **2014**, *28* (5), 585–587.
(10) Chabenne, J. R.; Mroz, P. A.; Mayer, J. P.; DiMarchi, R. D. Structural Refinement of Glucagon for Therapeutic Use. *J. Med. Chem.* **2020**, *63* (7), 3447–3460.
(11) Wang, Z.; Wang, J.; Li, H.; Yu, J.; Chen, G.; Kahkoska, A. R.; Wu, V.; Zeng, Y.; Wen, D.; Miedema, J. R.; Buse, J. B.; Gu, Z. Dual Self-Regulated Delivery of Insulin and Glucagon by a Hybrid Patch. *Proc. Natl. Acad. Sci. U. S. A.* **2020**, *117* (47), 29512–29517.
(12) Webber, M. J.; Appel, E. A.; Meijer, E. W.; Langer, R. Supramolecular Biomaterials. *Nat. Mater.* **2016**, *15* (1), 13–26.
(13) Webber, M. J.; Langer, R. Drug Delivery by Supramolecular Design. *Chem. Soc. Rev.* **2017**, *46* (21), 6600–6620.
(14) Webber, M. J. Engineering Responsive Supramolecular Biomaterials: Toward Smart Therapeutics. *Bioeng Transl Med* **2016**, *1* (3), 252–266.
(15) Sorrenti, A.; Leira-Iglesias, J.; Markvoort, A. J.; de Greef, T. F. A.; Hermans, T. M. Non-Equilibrium Supramolecular Polymerization. *Chem. Soc. Rev.* **2017**, *46* (18), 5476–5490.
(16) van Rossum, S. A. P.; Tena-Solsona, M.; van Esch, J. H.; Eelkema, R.; Boekhoven, J. Dissipative out-of-Equilibrium Assembly of Man-Made Supramolecular Materials. *Chem. Soc. Rev.* **2017**, *46* (18), 5519–5535.
(17) Hirst, A. R.; Roy, S.; Arora, M.; Das, A. K.; Hodson, N.; Murray, P.; Marshall, S.; Javid, N.; Sefcik, J.; Boekhoven, J.; van Esch, J. H.; Santabarbara, S.; Hunt, N. T.; Ulijn, R. V. Biocatalytic Induction of Supramolecular Order. *Nat. Chem.* **2010**, *2* (12), 1089–1094.
(18) Sorrenti, A.; Leira-Iglesias, J.; Sato, A.; Hermans, T. M. Non-Equilibrium Steady States in Supramolecular Polymerization. *Nat. Commun.* **2017**, *8*, 15899.
(19) Toledano, S.; Williams, R. J.; Jayawarna, V.; Ulijn, R. V. Enzyme-Triggered Self-Assembly of Peptide Hydrogels via Reversed Hydrolysis. *J. Am. Chem. Soc.* **2006**, *128* (4), 1070–1071.
(20) He, H.; Tan, W.; Guo, J.; Yi, M.; Shy, A. N.; Xu, B. Enzymatic Noncovalent Synthesis. *Chem. Rev.* **2020**, *120* (18), 9994–10078.
(21) Webber, M. J.; Newcomb, C. J.; Bitton, R.; Stupp, S. I. Switching of Self-Assembly in a Peptide Nanostructure with a Specific Enzyme. *Soft Matter* **2011**, *7* (20), 9665–9672.
(22) Chakroun, R. W.; Sneider, A.; Anderson, C. F.; Wang, F.; Wu, P.; Wirtz, D.; Cui, H. Supramolecular Design of Unsymmetric Reverse Bolaamphiphiles for Cell-Sensitive Hydrogel Degradation and Drug Release. *Angewandte Chemie*. 2020, pp 4464–4472. https://doi.org/10.1002/ange.201913087.
(23) Bankar, S. B.; Bule, M. V.; Singhal, R. S.; Ananthanarayan, L. Glucose Oxidase — An Overview. *Biotechnology Advances*. 2009, pp 489–501. https://doi.org/10.1016/j.biotechadv.2009.04.003.
(24) Podual, K.; Doyle, F. J., 3rd; Peppas, N. A. Glucose-Sensitivity of Glucose Oxidase-Containing Cationic Copolymer Hydrogels Having Poly(ethylene Glycol) Grafts. *J. Control. Release* **2000**, *67* (1), 9–17.
(25) Podual, K.; Doyle, F. J., III; Peppas, N. A. Dynamic Behavior of Glucose Oxidase-Containing Microparticles of Poly(ethylene Glycol)-Grafted Cationic Hydrogels in an Environment of Changing pH. *Biomaterials*. 2000, pp 1439–1450. https://doi.org/10.1016/s0142-9612(00)00020-x.
(26) Gu, Z.; Dang, T. T.; Ma, M.; Tang, B. C.; Cheng, H.; Jiang, S.; Dong, Y.; Zhang, Y.; Anderson, D. G. Glucose-Responsive Microgels Integrated with Enzyme Nanocapsules for Closed-Loop Insulin Delivery. *ACS Nano* **2013**, *7* (8), 6758–6766.
(27) Rodon Fores, J.; Martinez Mendez, M. L.; Mao, X.; Wagner, D.; Schmutz, M.; Rabineau, M.; Lavalle, P.; Schaaf, P.; Boulmedais, F.; Jierry, L. Localized Supramolecular Peptide Self-Assembly Directed by Enzyme-Induced Proton Gradients. *Angew. Chem. Int. Ed Engl.* **2017**, *56* (50), 15984–15988.
(28) Li, X.; Fu, M.; Wu, J.; Zhang, C.; Deng, X.; Dhinakar, A.; Huang, W.; Qian, H.; Ge, L. pH-Sensitive Peptide Hydrogel for Glucose-Responsive Insulin Delivery. *Acta Biomater.* **2017**, *51*, 294–303.
(29) Sis, M. J.; Webber, M. J. Drug Delivery with Designed Peptide Assemblies. *Trends Pharmacol. Sci.* **2019**, *40* (10), 747–762.
(30) Matson, J. B.; Zha, R. H.; Stupp, S. I. Peptide Self-Assembly for Crafting Functional Biological Materials. *Curr. Opin. Solid State Mater. Sci.* **2011**, *15* (6), 225–235.
(31) Cui, H.; Webber, M. J.; Stupp, S. I. Self-Assembly of Peptide Amphiphiles: From Molecules to Nanostructures to Biomaterials. *Biopolymers* **2010**, *94* (1), 1–18.
(32) Hartgerink, J. D.; Beniash, E.; Stupp, S. I. Self-Assembly and Mineralization of Peptide-Amphiphile Nanofibers. *Science* **2001**, *294* (5547), 1684–1688.
(33) Newcomb, C. J.; Sur, S.; Ortony, J. H.; Lee, O.-S.; Matson, J. B.; Boekhoven, J.; Yu, J. M.; Schatz, G. C.; Stupp, S. I. Cell Death versus Cell Survival Instructed by Supramolecular Cohesion of Nanostructures. *Nat. Commun.* **2014**, *5*, 3321.
(34) Velichko, Y. S.; Stupp, S. I.; de la Cruz, M. O. Molecular Simulation Study of Peptide Amphiphile Self-Assembly. *J. Phys. Chem. B* **2008**, *112* (8), 2326–2334.
(35) Xu, X.-D.; Jin, Y.; Liu, Y.; Zhang, X.-Z.; Zhuo, R.-X. Self-Assembly Behavior of Peptide Amphiphiles (PAs) with Different Length of Hydrophobic Alkyl Tails. *Colloids Surf. B Biointerfaces* **2010**, *81* (1), 329–335.
(36) Pashuck, E. T.; Cui, H.; Stupp, S. I. Tuning Supramolecular Rigidity of Peptide Fibers through Molecular Structure. *J. Am. Chem. Soc.* **2010**, *132* (17), 6041–6046.
(37) Stendahl, J. C.; Rao, M. S.; Guler, M. O.; Stupp, S. I. Intermolecular Forces in the Self-Assembly of Peptide Amphiphile Nanofibers. *Advanced Functional Materials*. 2006, pp 499–508. https://doi.org/10.1002/adfm.200500161.
(38) Cote, Y.; Fu, I. W.; Dobson, E. T.; Goldberger, J. E.; Nguyen, H. D.; Shen, J. K. Mechanism of the pH-Controlled Self-Assembly of Nanofibers from Peptide Amphiphiles. *J. Phys. Chem. C Nanomater. Interfaces* **2014**, *118* (29), 16272–16278.
(39) Webber, M. J.; Tongers, J.; Newcomb, C. J.; Marquardt, K.-T.; Bauersachs, J.; Losordo, D. W.; Stupp, S. I. Supramolecular Nanostructures That Mimic VEGF as a Strategy for Ischemic Tissue Repair. *Proc. Natl. Acad. Sci. U. S. A.* **2011**, *108* (33), 13438–13443.
(40) Carbonaro, M.; Nucara, A. Secondary Structure of Food Proteins by Fourier Transform Spectroscopy in the Mid-Infrared Region. *Amino Acids* **2010**, *38* (3), 679–690.
(41) Wilson, D.; Valluzzi, R.; Kaplan, D. Conformational Transitions in Model Silk Peptides. *Biophys. J.* **2000**, *78* (5), 2690–2701.
(42) Biancalana, M.; Makabe, K.; Koide, A.; Koide, S. Molecular Mechanism of Thioflavin-T Binding to the Surface of β-Rich Peptide Self-Assemblies. *Journal of Molecular Biology*. 2009, pp 1052–1063. https://doi.org/10.1016/j.jmb.2008.11.006.
(43) Yan, C.; Pochan, D. J. Rheological Properties of Peptide-Based Hydrogels for Biomedical and Other Applications. *Chem. Soc. Rev.* **2010**, *39* (9), 3528–3540.
(44) Sahoo, J. K.; VandenBerg, M. A.; Webber, M. J. Injectable Network Biomaterials via Molecular or Colloidal Self-Assembly. *Adv. Drug Deliv. Rev.* **2018**, *127*, 185–207.
(45) Chen, M. H.; Wang, L. L.; Chung, J. J.; Kim, Y.-H.; Atluri, P.; Burdick, J. A. Methods To Assess Shear-Thinning Hydrogels for Application As Injectable Biomaterials. *ACS Biomater Sci Eng* **2017**, *3* (12), 3146–3160.
(46) Hövelmann, U.; Bysted, B. V.; Mouritzen, U.; Macchi, F.; Lamers, D.; Kronshage, B.; Møller, D. V.; Heise, T. Pharmacokinetic and Pharmacodynamic Characteristics of Dasiglucagon, a Novel Soluble and Stable Glucagon Analog. *Diabetes Care* **2018**, *41* (3), 531–537.
(47) Gu, Z.; Aimetti, A. A.; Wang, Q.; Dang, T. T.; Zhang, Y.; Veiseh, O.; Cheng, H.; Langer, R. S.; Anderson, D. G. Injectable Nano-Network for Glucose-Mediated Insulin Delivery. *ACS Nano* **2013**, *7* (5), 4194–4201.
(48) Blevins, T. C. Professional Continuous Glucose Monitoring in Clinical Practice 2010. *J. Diabetes Sci. Technol.* **2010**, *4* (2), 440–456.
(49) Capozzi, M. E.; Wait, J. B.; Koech, J.; Gordon, A. N.; Coch, R. W.; Svendsen, B.; Finan, B.; D'Alessio, D. A.; Campbell, J. E. Glucagon Lowers Glycemia When β Cells Are Active. *JCI Insight*. 2019. https://doi.org/10.1172/jci.insight.129954.
(50) Havelund, S.; Plum, A.; Ribel, U.; Jonassen, I.; Vølund, A.; Markussen, J.; Kurtzhals, P. The Mechanism of Protraction of Insulin Detemir, a Long-Acting, Acylated Analog of Human Insulin. *Pharm. Res.* **2004**, *21* (8), 1498–1504.
(51) Ghanaati, S.; Webber, M. J.; Unger, R. E.; Orth, C.; Hulvat, J. F.; Kiehna, S. E.; Barbeck, M.; Rasic, A.; Stupp, S. I.; Kirkpatrick, C. J. Dynamic in Vivo

Biocompatibility of Angiogenic Peptide Amphiphile Nanofibers. *Biomaterials* **2009**, *30* (31), 6202–6212.

(52) Yu, J.; Zhang, Y.; Sun, W.; Kahkoska, A. R.; Wang, J.; Buse, J. B.; Gu, Z. Insulin-Responsive Glucagon Delivery for Prevention of Hypoglycemia. *Small* **2017**, *13* (19). https://doi.org/10.1002/smll.201603028.

(53) GhavamiNejad, A.; Li, J.; Lu, B.; Zhou, L.; Lam, L.; Giacca, A.; Wu, X. Y. Glucose-Responsive Composite Microneedle Patch for Hypoglycemia-Triggered Delivery of Native Glucagon. *Adv. Mater.* **2019**, *31* (30), e1901051.

(54) El-Khatib, F. H.; Balliro, C.; Hillard, M. A.; Magyar, K. L.; Ekhlaspour, L.; Sinha, M.; Mondesir, D.; Esmaeili, A.; Hartigan, C.; Thompson, M. J.; Malkani, S.; Lock, J. P.; Harlan, D. M.; Clinton, P.; Frank, E.; Wilson, D. M.; DeSalvo, D.; Norlander, L.; Ly, T.; Buckingham, B. A.; Diner, J.; Dezube, M.; Young, L. A.; Goley, A.; Kirkman, M. S.; Buse, J. B.; Zheng, H.; Selagamsetty, R. R.; Damiano, E. R.; Russell, S. J. Home Use of a Bihormonal Bionic Pancreas versus Insulin Pump Therapy in Adults with Type 1 Diabetes: A Multicentre Randomised Crossover Trial. *Lancet* **2017**, *389* (10067), 369–380.

(55) Chou, D. H.-C.; Webber, M. J.; Tang, B. C.; Lin, A. B.; Thapa, L. S.; Deng, D.; Truong, J. V.; Cortinas, A. B.; Langer, R.; Anderson, D. G. Glucose-Responsive Insulin Activity by Covalent Modification with Aliphatic Phenylboronic Acid Conjugates. *Proc. Natl. Acad. Sci. U. S. A.* **2015**, *112* (8), 2401–2406.

Insert Table of Contents artwork here

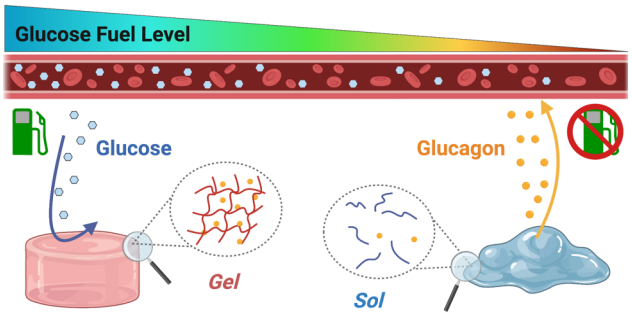

Synopsis: Enzymatic control of molecular self-assembly and hydrogelation enables encapsulation and glucose-responsive delivery of a therapeutic to address low glucose.